Journal of American Chemical Society, Submitted: September 30, 2002

Surface Chemistry on Bimetallic Alloy Surfaces: Adsorption of Anions and Oxidation of CO on $Pt_3Sn(111)$

V. Stamenković, M. Arenz, C A Lucas[+], M. E. Gallagher[+], P N. Ross, N M. Marković[*]

Materials Sciences Division Lawrence Berkeley National Laboratory
University of California, Berkeley, CA 94720
Oliver Lodge Laboratory, Department of Physics, University of Liverpool,
Liverpool, L69 7ZE, UK [+]

Abstract:

The microscopic structure of the $Pt_3Sn(111)$ surface in an electrochemical environment has been studied by a combination of ex-situ low energy electron diffraction (LEED), Auger electron spectroscopy (AES) and low energy ion scattering (LEIS) and in-situ surface X-ray scattering (SXS) and Fourier transform infrared (FTIR) spectroscopy. In ultra high vacuum (UHV) the clean-annealed surface produces a p(2 x 2) LEED pattern consistent with the surface composition, determined by LEIS, of 25 at% Sn. SXS results show that the p(2 x 2) structure can be "transferred" from UHV into 0.5 M H_2SO_4 and that the surface structure remains stable from 0.05 to 0.8 V. At 0.05 V the expansion of Pt surface atoms, ca. +2% from the bulk lattice spacing, is induced by adsorption of underpotential deposited (UPD) hydrogen. At 0.5 V, where Pt atoms are covered by (bi)sulfate anions, the topmost layer is contracted relative to 0.05 V, although Sn atoms expend significantly, ca 8.5%. The p(2 x 2) structure is stable even in solution containing CO. In contrast to the Pt(111)-CO system, no ordered structures of CO are formed on the $Pt_3Sn(111)$ surface and the topmost layer expands relatively little (ca. 1.5%) from the bulk lattice spacing upon the adsorption of CO. The binding site geometry of CO on $Pt_3Sn(111)$ is determined by FTIR. In contrast to the near invariant

[*]Corresponding author:
e-mail: nmmarkovic@lbl.gov

bandshape of a-top CO on Pt(111), changes in band morphology (splitting of the band) and vibrational properties (increase in the frequency mode) are clearly visible on the $Pt_3Sn(111)$ surface. In order to explain the lineshape of the CO bands we suggest that in addition to alloying effects, other factors, such as intermolecular repulsion between co-adsorbed CO and OH species, are controlling segregation of CO into cluster domains where the local CO coverage is different from the coverage expected for the CO-CO interaction on an unmodified Pt(111) surface.

1. Introduction

For over a decade now the ability to characterize atomic/molecular spatial structures and to monitor changes in the local symmetry of surface atoms in-situ under the reaction conditions has played an important part in our understanding of surface electrochemistry at metal-based interfaces. This progress has been influenced greatly by the development of in-situ surface sensitive probes [1-8] and vibrational spectroscopes [9-12], which in combination with classical electrochemical methods [13-15] have been used to find interrelationships between the microscopic surface structures of fcc metals (Pt, Ir, Pd, Au, Ag, Cu) and the macroscopic kinetic rates of the reactions. As for pure metals, considerable effort has also been directed to the study of surface electrochemistry on well-characterized Pt-bimetallic surfaces, which can be prepared either by deposition of one metal on the surface of another [16;17] or, using conventional metallurgy, as bulk alloys [18;19]. While for the former systems significant progress has been made [15], for the bulk alloys there is still much to be understood regarding both adsorptive chemistry and electrocatalytic properties at the atomic levels.

$Pt_3Sn(111)$ is one of the most active systems known for CO oxidation. In this paper we attempt to provide insight of the macroscopic level descriptions of the $Pt_3Sn(111)$ surface in the electrochemical environment via atomic level characterization. First the structural properties of the $Pt_3Sn(111)$ surface in electrolyte are examined by SXS, including both the stability of the UHV-prepared p(2x2) structure in sulfuric acid solution and the potential-dependent relaxation of Pt and Sn atoms in the near-surface region. Adsorption of sulfuric acid anions on the p(2 x 2) phase is examined by FTIR spectroscopy. These results unambiguously show that the puzzling pseudocapacitance in the cyclic voltammetry of $Pt_3Sn(111)$ is associated with adsorption/desorption of (bi)sulfate anions on Pt sites. During

electrochemical oxidation of CO on the p(2 x 2) surface *in-situ* SXS and FTIR are used to show (explain) why $Pt_3Sn(111)$ is so active for this reaction.

2. Experimental

The $Pt_3Sn(111)$ single crystal was prepared by a procedure which has been fully described in ref. [19;20], i.e. by combining high-purity platinum and tin in stoichiometric amounts and then refining the alloy using the Bridgeman-Stockberger technique under a helium atmosphere in a high-purity alumina crucible. The composition of the intermetallic compound was confirmed by quantitative analysis using wet chemical method and emission spectroscopy (Galbraith Laboratories) to be 24.3±0.5% Sn. A single crystal slice oriented along (111) was spark-cut to be 4mm x 6 mm diameter and then mechanically polished to 0.05μm. The single crystal face was within 0.5° of its respective crystal planes as determined by Laue back reflection x-ray diffraction.

2.1 UHV surface preparation and characterization

The $Pt_3Sn(111)$ surface was prepared and characterized in a UHV system, with a base pressure of $2 \cdot 10^{-10}$ Torr range, equipped with an angular-resolving double pass cylindrical mirror analyzer PHI-DPCMA Φ15-255GAR with an electron source at its center. The surface was clean done by repeated cycles of sputter-annealing cycles until Auger electron spectroscopy (AES) indicated that a perfectly clean (carbon and oxygen free) surface was produced. AES spectra (Figure 1a) were recorded in derivative mode using the 3 keV electron beam energy, 3 eV_{p-p} modulation and –5 μA beam current in the range from 140 to 600 eV. The LEED pattern following Ar^+ bombardment and annealing is shown in Figure 1c. In agreement with reference [21], the clean-annealed surface produced half-order spots in the LEED

pattern, characteristic of the p(2 x 2) structure that is observed on other alloys having the same Ll_2 structure as Pt_3Sn [22]. A real space model for the p(2 x 2) surface is depicted in Figure 1.

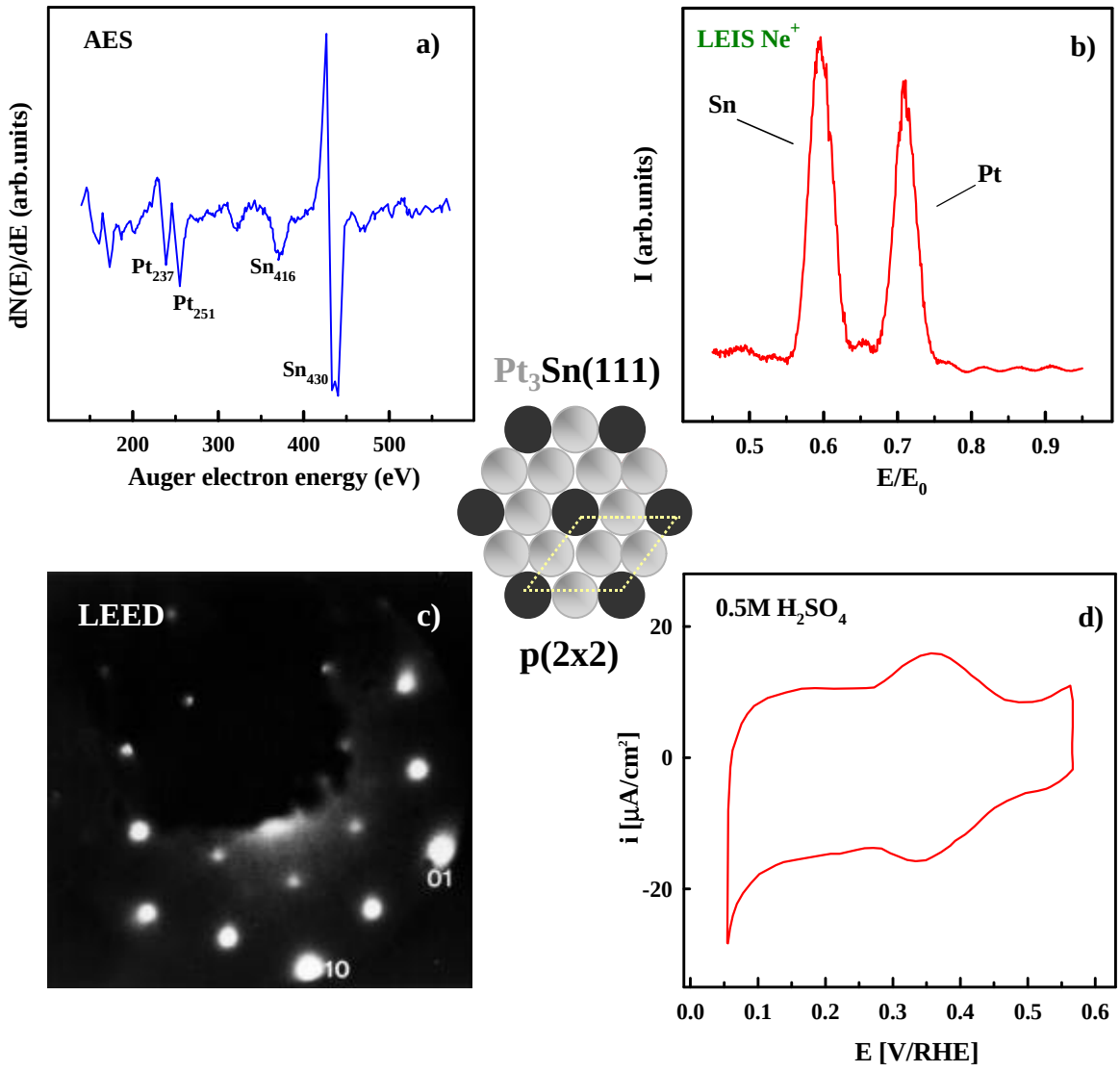

Figure 1. Surface characterization of the $Pt_3Sn(111)$ in UHV: **(a)** AES, **(b)** LEIS, **(c)** LEED and **(d)** cyclic voltammetry in 0.5 M H_2SO_4. Model is schematic representation of the observed p(2x2) LEED pattern.

After mild sputtering (with a 0.5 keV beam of Ar^+ ions) and annealing at 1000K the surface composition was determined by low energy ion scattering (LEIS), see Figure 1b. LEIS spectra were taken with a Ne^+ beam energy of 1 keV with sample current from 5 to 30 nA at residual Ne pressure of $2.5 \cdot 10^{-8}$ Torr. The scattering angle was 127° and the incidence angle was 45°.

A Φ04-303A differentially pumped ion gun was used to raster the Ne^+ ion beam over a 3 mm × 3 mm area. Using the theoretical ion-scattering cross-sections for Sn and Pt [23], the LEIS spectrum indicates that the surface composition is 25 at% Sn and 75% of Pt, consistent with the p(2 x 2) LEED pattern and bulk truncation of the surface structure.

2.2 Electrochemical measurements

The UHV prepared and characterized $Pt_3Sn(111)$ surface was transferred from the UHV introductory port (back-filled with argon) and covered immediately with a drop of triply pyro-distilled water, for details see [24]. The electrode was then mounted in a rotating disk electrode and finally immersed in electrolyte under potential control at ~0.05V vs RHE in 0.5M H_2SO_4 (Baker, Ultrex). A typical cyclic voltammetry of the $Pt_3Sn(111)$ in supporting electrolyte is shown in Figure 1d. The reference electrode was a saturated calomel electrode (SCE) separated by a bridge from the reference compartment. All potentials in this paper are, however, referenced to the reversible hydrogen electrode potential (RHE) at the same temperature (calibrated from the hydrogen oxidation reaction [25]) in the same electrolyte; argon, was bubbled through a glass frit (Air Products, 5N8 purity). The geometrical surface area of the disk electrode was 0.283 cm^2, and all voltammograms were recorded with a sweep rate of either 50 mV/s or 20 mV/s.

2.3 FTIR measurements

The in situ FTIR measurements were taken with a Nicolet Nexus 670 spectrometer purged with nitrogen and equipped with a MCT detector cooled with liquid nitrogen. All IR measurements were performed in a spectroelectrochemical glass cell designed for an external reflection mode in a thin layer configuration. The cell is coupled at its bottom with a CaF_2 prism beveled at 60° from the surface normal. Prior to each measurement a cyclic voltammogram was recorded in order to confirm the cleanliness of the electrode surface.

Subsequently the solution was saturated with CO for at least 3 min. holding the electrode potential at 0.05 V. The spectra were recorded with a resolution of 8 cm^{-1}. All measurements were performed using p-polarized light. In order to obtain a single beam spectrum 50 scans were collected at each potential resulting in a recording time of 25 s. Absorbance spectra were calculated as the ratio $-\log(R/R_0)$ where R and R_0 are the reflectance values corresponding to the sample and reference spectra, respectively. Reference spectra were recorded either at 0.9 V or –0.05 V, where CO_{ad} is completely oxidized and before the onset of CO_{ad} oxidation, respectively. The reference potential in the spectroelectrochemical cell was controlled by a reversible hydrogen electrode (RHE).

2.4 SXS measurements

The general experimental procedure used in X-ray diffraction measurements of electrochemical systems has been described in detail in previous articles [4-6]. As for electrochemical measurements, the UHV-prepared and characterized $Pt_3Sn(111)$ crystal (miscut $<0.1^0$) was transferred into the X-ray electrochemical cell. The cell was mounted at the center of a four-circle Huber goniometer on beamline 7-2 at the Stanford Synchrotron Radiation Laboratory (SSRL), using a 10 keV x-ray beam, defined by slits to be a 1mm x 1mm spot at the sample. Diffracted X-rays were measured by a Ge solid state detector after passing through a Soller slit which defined an in-plane resolution of ca. 0.005 $Å^{-1}$. The crystal was indexed to the conventional hexagonal unit cell for the (111) surface. Further experimental details can be found in references [26].

3. Results and Discussion

3.1 Surface characterization of $Pt_3Sn(111)$: LEED, CV and SXS

The ability to characterize atomic/molecular spatial structures and to monitor changes in the local symmetry of surface atoms in-situ under reaction conditions has played an

important part in surface electrochemistry at monocrystalline metal electrodes. For example, we used SXS to demonstrate that the (1 x 1) surface of Pt(111), prepared by a flame annealing method [27;28], remains stable upon contact with aqueous solutions or even when the potential is cycled between the hydrogen evolution and the oxide formation potential regions. There have been no studies, however, which could provide such links between the in-situ surface structure/composition of bulk alloys and their adsorptive chemistry. As for Pt(111), in the present work we have also used SXS to establish whether the p(2x2) structure, observed by LEED in Figure 1c, remains stable in 0.5 M H_2SO_4. From the fact that upon contact with solution at 0.05 V the $Pt_3Sn(111)$ surface remains flat and terminated by the bulk structure, we conclude the p(2x2) structure of Sn can indeed be "transferred" from a UHV system to an electrochemical environment (!). Equally important, even when the electrode potential was cycled from hydrogen adsorption up to 0.6 V, the p(2x2) structure remained stable with the surface composition expected for the bulk termination surface structure (e.g. 25 at% Sn). The important consequence of the structure/composition stability of $Pt_3Sn(111)$ in 0.5 M H_2SO_4 is that the interpretation of the cyclic voltammetry of $Pt_3Sn(111)$ in argon-purged 0.5 M H_2SO_4, depicted in Figure 2a, can be based on the adsorption sites available on the p(2 x 2) surface, see model in Figure 1. Notice that the H_{upd} pseudocapacitance ($0.05 < E < \approx 0.25\text{-}0.35$ V) is considerably reduced from that of the corresponding Sn-free Pt(111) surface (see dotted curve in Figure 2a), as one might expect from an alloying element (Sn) that does not adsorb hydrogen [20]. Further inspection of Figure 2 clearly reveals that the H_{upd} potential region on $Pt_3Sn(111)$ is followed with a puzzling reversible feature ($0.25 E < 0.5$ V) which could be produced by any number of processes including hydrogen adsorption, bisulfate adsorption, OH adsorption and/or a Sn surface redox process [19]. In the next section, the nature of the "anomalous" feature in the cyclic voltammetry of $Pt_3Sn(111)$ will be probed by means of FTIR spectroscopy.

3.2 Bisulfate adsorption on $Pt_3Sn(111)$: FTIR measurements

After more than two decades of controversy, it is now well established that the reversible "anomalous" feature observed in the CV of Pt(111) in sulfuric acid solutions between 0.35 to 0.65 V (Figure 2b) is due to adsorption/desorption of bisulfate anions.

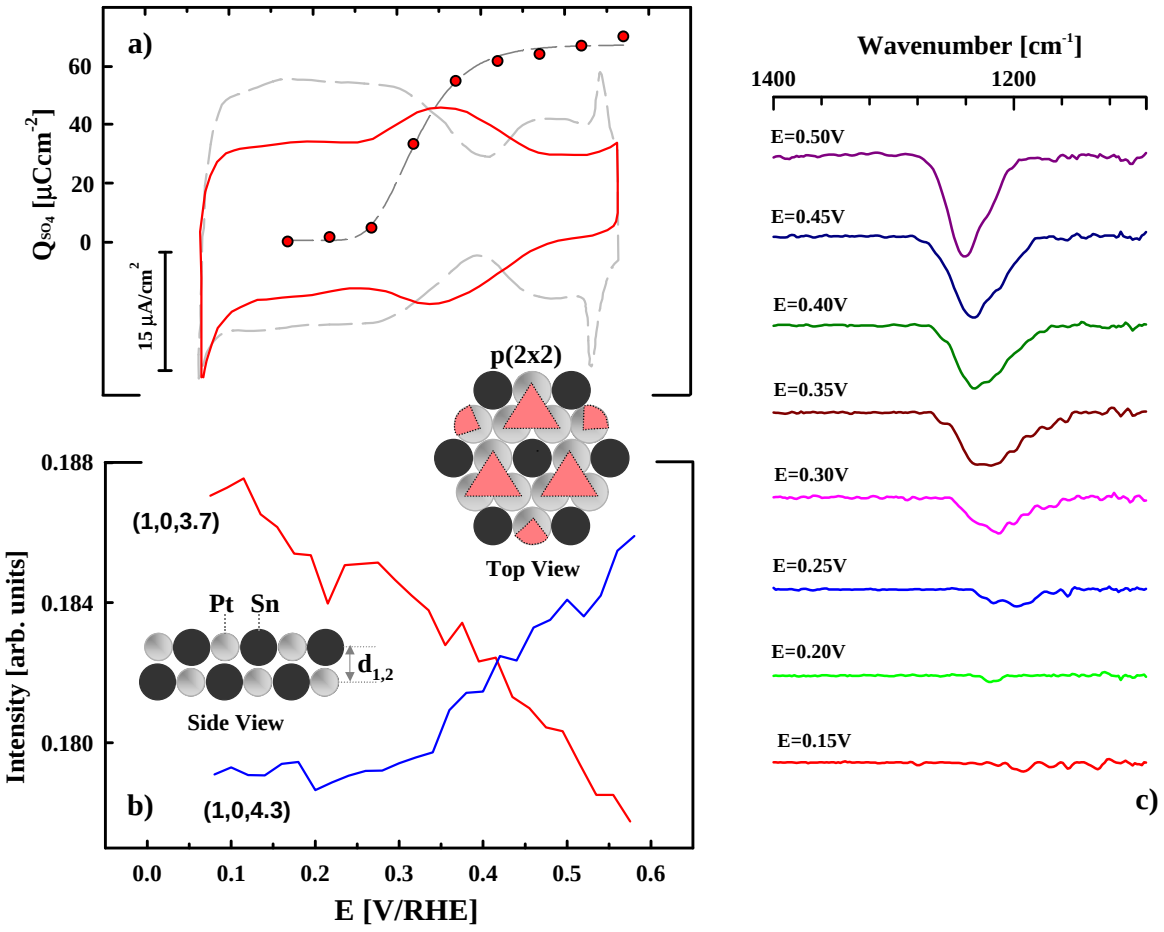

Figure 2. (a) Cyclic voltammograms of Pt(111) (dashed gray line) and $Pt_3Sn(111)$ (solid red line) in 0.5 M H_2SO_4. Potential dependent integrated charges for the adsorption of (bi) sulfate anions on the $Pt_3Sn(111)$ surface are represented by circles. **(b)** The measured x-ray intensities at (1,0,3.7) and (1,0,4.3) as a function of the electrode potentials. Top and side views represent of the proposed p(2x2) structure. The gray circles are Pt surface atoms, the black circles are Sn atoms and triangles are (bi) sulfate anions which are adsorbed on Pt sites. The side view indicates the surface normal spacing that are derived from the CTR measurements. **(c)** IRAS spectra of (bi)sulfate anions adsorbed at $Pt_3Sn(111)$ recorded as the potential was stepped in sequence from –0.05 to 0.65 V.

The first evidence was obtained from FTIR spectroscopy [9;11;12], then from radiotracer measurements [29;30], chronocoulonometric measurements [31] and finally from STM experiments [32]. As for the Pt(111)-bisulfate system, FTIR characterization of the $Pt_3Sn(111)$ alloy in sulfuric acid solution is used to establish whether the origin of the "anomalous" feature in the voltammetry of Figure 2a also arises from bisulfate adsorption/desorption. Figure 2b shows sets of spectra obtained for the $Pt_3Sn(111)$ alloy in 0.5 M H_2SO_4 over the potential range from hydrogen evolution to just before the onset of Sn dissolution. A negative going band is clearly visible in the spectra at a potential near to the onset (ca. at 0.2 V) of the formation of the puzzling pseudocapacitance in Figure 2a. The band at low potentials is broad and weak with the peak position centered at ca. 1210 cm^{-1}. As the potential is scanned positively the band becomes more intense and at 0.5 V the peak position shifts to ca. 1240 cm^{-1}. Interestingly, very similar FTIR spectra were recorded for the adsorption of (bi)sulfate[1] anions on Pt(111) [9]. This similarity is not coincidental and can be used as conformation that the "anomalous" feature observed in the CV of $Pt_3Sn(111)$ corresponds to (bi)sulfate anion adsorption *at* Pt sites. The recognition that FTIR spectra for bisulfate adsorption on Pt(111) in refs. [9] are almost identical with those depicted in Figure 2b also suggests that Sn atoms have only a small effect on the active Pt-(bi)sulfate bands. The potential-dependent surface coverage of (bi)sulfate anions on the $Pt_3Sn(111)$ surface, obtained by integrating the charge under the pseudocapacitance between 0.2 to 0.5 V, is plotted in Figure 1a. The total charge passing the interface in this potential region is ca. 65 $\mu C/cm^2$, or about 75 % of that of the corresponding

[1] For the Pt(111)-bisulfate system, there has been some controversy about the assignment of the adsorbed bands for sulfuric acid anion. Initially, Feguy et al assigned this band to an SO_3 asymmetric stretching mode of bisulfate anions which are adsorbed on the Pt atoms via the three unprotonated oxygen atoms.. Subsequent studies by other groups have disputed this interpretation and the same band was assigned to a symmetric SO_3 stretch of bisulfate anions [9] or to the S-O stretch of non-coordinated SO group of the adsorbed sulfate anion. To reconcile these two extremes, Faguy et al. recently suggested that the adsorbate in the anomalous potential region is a H_3O^+-SO_4^{2-} species [70]. We consider the issue unresolved and thus refer to adsorbing species on Pt(111) in the "butterfly" region equivocally as (bi)sulfate.

Sn-free Pt(111) surface (≈80 μC/cm). Thus, the charge for the (bi)sulfate adsorption on the former surface is reduced ≈25 % from the charged required to form a close-packed layer of (bi)sulfate anions on the Pt(111) surface, or simply by the amount of Sn atoms present in the p(2 x 2) structure. This suggests that (bi) sulfate anions are not adsorbed on Sn atoms. A representation of a possible structure model for (bi)sulfate adsorption on the p(2 x 2) $Pt_3Sn(111)$ surface is depicted in Figure 1. Based on this model a tetrahedral (bi)sulfate anion is adsorbed on Pt atoms via the three oxygen atoms, as proposed for the (bi)sulfate interaction with the Pt(111) surface [33].

Further inspection of Figure 2a reveals that adsorption of (bi)sulfate anions on $Pt_3Sn(111)$ takes place at more negative potentials than on Pt(111), ca. 0.15 V. An enhancement of anion adsorption on Pt(111) modified with admetals is not surprising and it has been observed previously in radiotracer work by Wieckowski and co-workers for the Pt-Cu_{upd} system [34], and by Lipkowski and coworkers for the Au(111)-Cu_{upd} systems [35;36], as well as by our group for the Pt-Cu_{upd} [37;38], Pt-Pb_{upd} and Pt-Bi_{upd} [39;40] systems. We suggested a mechanism for this induced anion adsorption in terms of the local work function concept and the local pzc effect [41]. This concept has been discussed previously [39;42-44], so the remarks here are correspondingly brief. Modifying Pt with Cu and Pb adatoms lowers the work function of Pt atoms within a Fermi-Thomas screening length of the admetal, resulting in more anion adsorption at these sites at the given electrode potential than on the sites which are not affected by the UPD adatoms. Using the same argument for the Pt-Sn system, adsorption of (bi)sulfate anions on the $Pt_3Sn(111)$ surface is observed at a lower electrode potential than on an unmodified Pt(111) surface because Sn lowers the work function of the Pt atoms.

3.3 Adsorbate induced structure changes

Having established the window of stability of the p(2x2) structure in electrolyte, additional structure details, such as adsorbate induced surface relaxation, were examined by analyzing crystal truncation road (CTR)[2] data [1-3;45]. Selected results from that study are, however, given here in order to provide a complete picture of the $Pt_3Sn(111)$ surface in electrolyte under reaction conditions. In particular, measurements of x-ray intensity changes at (1, 0, 3.6) and (1, 0, 4.3), reciprocal lattice points where the scattered intensity is sensitive to surface relaxation effects, of $Pt_3Sn(111)$ in 0.5 M H_2SO_4 solution as the function of the applied potential (termed as x-ray voltammetry, XRV [46]) are shown in Figure 2b. The fact that the X-ray intensities at these two reciprocal lattice points show "mirror-like" behavior as the potential is scanned is consistent with a surface relaxation effect rather than surface roughening. Close inspection of the XRV results in Figure 2b reveals that the desorption of hydrogen as well as the adsorption of bisulfate anions lead to contraction of the surface atoms, i.e. Δd interplanar spacing in the insert of Figure 2b decreases monotonically by scanning the potential positively from 0.05 V. In line with previous studies [4], analysis of the relevant CTR data has been performed in order to extract the detailed structural parameters for the $Pt_3Sn(111)$ surface in electrolyte. From fits to the CTR data, using a structural model in which the vertical displacement (Δd_{Pt}, Δd_{Sn}), surface coverage (Θ_{Pt},Θ_{Sn}) and roughness (σ_{Pt},σ_{Sn}) of the Pt and Sn in the topmost two layers were allowed to vary independently. The results indicated two important characteristics of the surface structure at 0.05 V: (i) expansion of the surface Pt atoms induced by the adsorption of hydrogen is very similar to that observed on Pt(111) [46;47] (Δd^1_{Pt} = = +2%); and (ii) the expansion of Sn surface atoms with increasing potential is larger than with Pt atoms (which actually contract when H_{upd} is oxidized). At 0.55V Sn atoms remain

[2] CTR are rods of scattering which are aligned along the surface normal in the $Pt_3Sn(111)$ reciprocal space and pass through bulk Bragg reflections [45].

in the p(2x2) structure and Pt surface atoms are unrelaxed, while the Sn atoms in the topmost layer expand up to Δd_{Sn}^{1}=8.5% of the lattice spacing. At potentials higher than 0.5 V, this expansion is even more pronounced, indicating that before Sn dissolution the Sn surface atoms are expanded by ca. 12% of the bulk lattice spacing.

3.4 CO oxidation on $Pt_3Sn(111)$: Surface structures under reaction conditions

The electrooxidation of CO on $Pt_3Sn(hkl)$ surfaces occupies an important position in surface electrochemistry. Concentrating on both catalytic activity and structure sensitivity, Gasteiger et al demonstrated that $Pt_3Sn(hkl)$ single crystals have the highest catalytic activity for CO oxidation ever found at the metal-liquid interface in acid solutions [20]. The most active surface was found to be $Pt_3Sn(111)$, an alloy on which the onset potential for the continuous oxidation of dissolved CO (ca. 0.2 V in Figure 3a) is shifted negatively with respect to that for the $Pt_3Sn(110)$ surface by about 0.1 V and by ≈0.45 V with respect to pure Pt. It was proposed that the significant enhancement produced by alloying Pt with Sn atoms can be ascribed to a combination of both bifunctional and ligand (electronic effects) effects [19;20].

In the bifunctional effect, Sn nucleates oxygenated species[3] which then react with the adsorbed CO (hereafter denoted as CO_{ad}) on Pt atoms [20],

$$Pt - CO_{ad} + Sn - OH_{ad} = CO_2 + H^+ + e^- \qquad (1)$$

This mechanism is consistent with the positive reaction order with the respect to the partial pressure of dissolved CO (hereafter denoted as CO_b). In agreement with experimental observations, from the calculated binding energies of CO and OH on the $Pt_3Sn(111)$ surface it was found that while CO does not bind to the Sn, OH_{ad} clearly shows a preference for the Sn

[3] As discussed bellow the true nature of oxygenated species adsorbed on Sn is still unknown, e.g. Sn atoms in the Pt-Sn alloy may have multiple oxygenated ligands, the stoichiometry of which may vary with the potential. For the sake of simplicity, however, in the further discussion these oxygenated species will simply be assigned as OH_{ad}.

atop coordination surface atoms [48]. On the other hand, the ligand effect, where the second component (Sn atoms) may alter the electronic properties of catalytically active metal (Pt atoms), is a consequence of the strong intermetallic bonding between Pt and Sn.

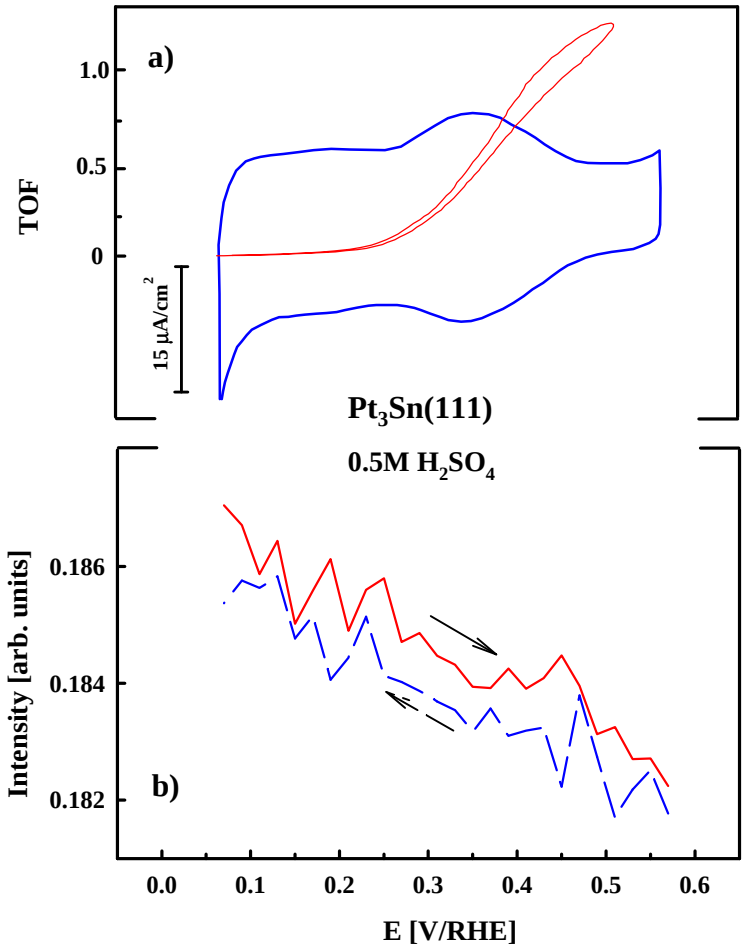

Figure 3. **(a)** Cyclic voltammogram of the $Pt_3Sn(111)$ in 0.5 M H_2SO_4 and corresponding polarization curve for the CO oxidation dissolved (1atm) in solution. **(b)** The measured x-ray intensities at (1,0,3.7) as a function of the electrode potentials in 0.5 M H_2SO_4 saturated with CO.

The ligand effect is multifaceted, including the formation of the so-called "weakly" adsorbed state of CO_{ad} [20;49](denoted as CO_{ad}^{w}) on Pt sites as well as an increased stability of Sn atoms in the Pt_3Sn surface [20]. Due to lack of any atomic-level structure information in our early work, we could only characterize the CO_{ad}^{w} state thermodynamically, i.e. CO_{ad}, with a low heat of

adsorption. In what follows, by a combination of SXS and FTIR measurements this macroscopic description of the CO_{ad}^{w} state will be elevated to a microscopic level, that enables the relation between reactivity and the interfacial structure of CO_{ad} on $Pt_3Sn(111)$ to be understood.

3.4.1 SXS measurements

Direct information regarding the CO_{ad} structure and stability of the p(2 x 2) phase in the presence of CO_b was established by using SXS. The p(2 x 2) structure remains stable in a solution containing CO and the potential window of stability appears to be even wider than in CO-free solution, i.e. between $0.05 < E < 0.9$ V. As a consequence, the polarization curve for CO oxidation, shown in Figure 2a, corresponds to CO_{ad} oxidation on a well-ordered $Pt_3Sn(111)$ surface. Unfortunately, in contrast to the Pt(111)-CO system [46;49] it was not possible to detect ordered structures of CO on the $Pt_3Sn(111)$ surface by SXS.

The expansion of surface atoms upon the adsorption of CO on the $Pt_3Sn(111)$ surface (CO is exclusively adsorbed on Pt sites [20]) is ca.1.5%, which is significantly smaller than the ca. 4% expansion induced by the adsorption of CO on Pt(111) [46;50]. The difference in relaxation of Pt(111) and $Pt_3Sn(111)$ surface layers covered with CO most likely arises from the difference in the adsorbate0-metal bonding, the Pt(111)-CO interaction being stronger than the $Pt_3Sn(111)$-CO. This observation provides a first independent conformation of the existence of the "weakly" adsorbed state of CO on the $Pt_3Sn(111)$ surface, originally proposed by our group [20] and later supported by density functional theory (DFT) calculations [48]. The DFT calculations indicated that CO binds only to Pt atoms (with binding energy of –1.41 eV vs –1.20 eV for the pure Pt) and not to the Sn atom, whereas OH has an energetic preference for the Sn sites (with binding energy of –2.66 eV).

Direct information regarding the induced relaxation of surface Pt and Sn atoms by the adsorption of CO are obtained by analyzing and modeling CTR data. Those results for the $Pt_3Sn(111)$-CO system indicated that the measurements were insensitive to both the CO adlayer (formed on Pt ensembles of the p(2x2) structure) and the oxygenated species (present on Sn atoms) due to the relatively weak scattering power of C, O and H atoms compared to Pt and Sn atoms. Using the same structural model used to describe the $Pt_3Sn(111)$ surface in the absence of CO two general features emerge from the CRT results: while at 0.05 V both Pt and Sn atoms are expanded relatively little from the bulk lattice spacing (ca. 1.5%), at 0.5 V the expansion of Pt atoms remains the same as at low potentials, in contrast to significant expansion of the Sn atoms from the second layer, ca. 6%. Although Sn atoms are highly expanded from the bulk lattice position, the XRV in Figure 3b shows that upon sweeping the potential positively from 0.05 V the oxidation of CO is associated with a net contraction of the surface layer, consistent with our previous remarks that the relaxation of the topmost *layer* at positive potentials is predominantly controlled by the contraction of the majority Pt rich (75 at %) surface atoms.

3.4.2 FTIR measurements

The binding site occupancy of CO on the $Pt_3Sn(111)$ surface was obtained by utilizing FTIR spectroscopy, shown previously for the interaction of CO with the Pt(111) surface [50]. Figure 4 shows a set of the CO absorbance spectra referred to the single beam spectrum collected at 0.65 V. The assignment of CO adsorption sites on $Pt_3Sn(111)$ can best be done by comparing the present data to those from the system Pt(111)-CO_{ad}, the latter being described in detail by many groups [51-54]. From Figure 4 and references [50;52], therefore, it is clear that neither on atop/three-fold-hollow nor an atop/bridge combination of CO_{ad}, which are characteristic for the Pt(111)-CO system, are observed at the $Pt_3Sn(111)$ surface. In addition, in contrast to the

near invariant bands of a-top CO on Pt(111) [50], changes in the band shape (splitting of the band) and frequency are clearly visible on the $Pt_3Sn(111)$ surface, e.g., pair of bands centered at ca. 2090 and 2077 cm^{1-} (at low potentials) are transformed into a single relatively broad peak centered at ca. 2077 cm^{-1} at higher potentials.

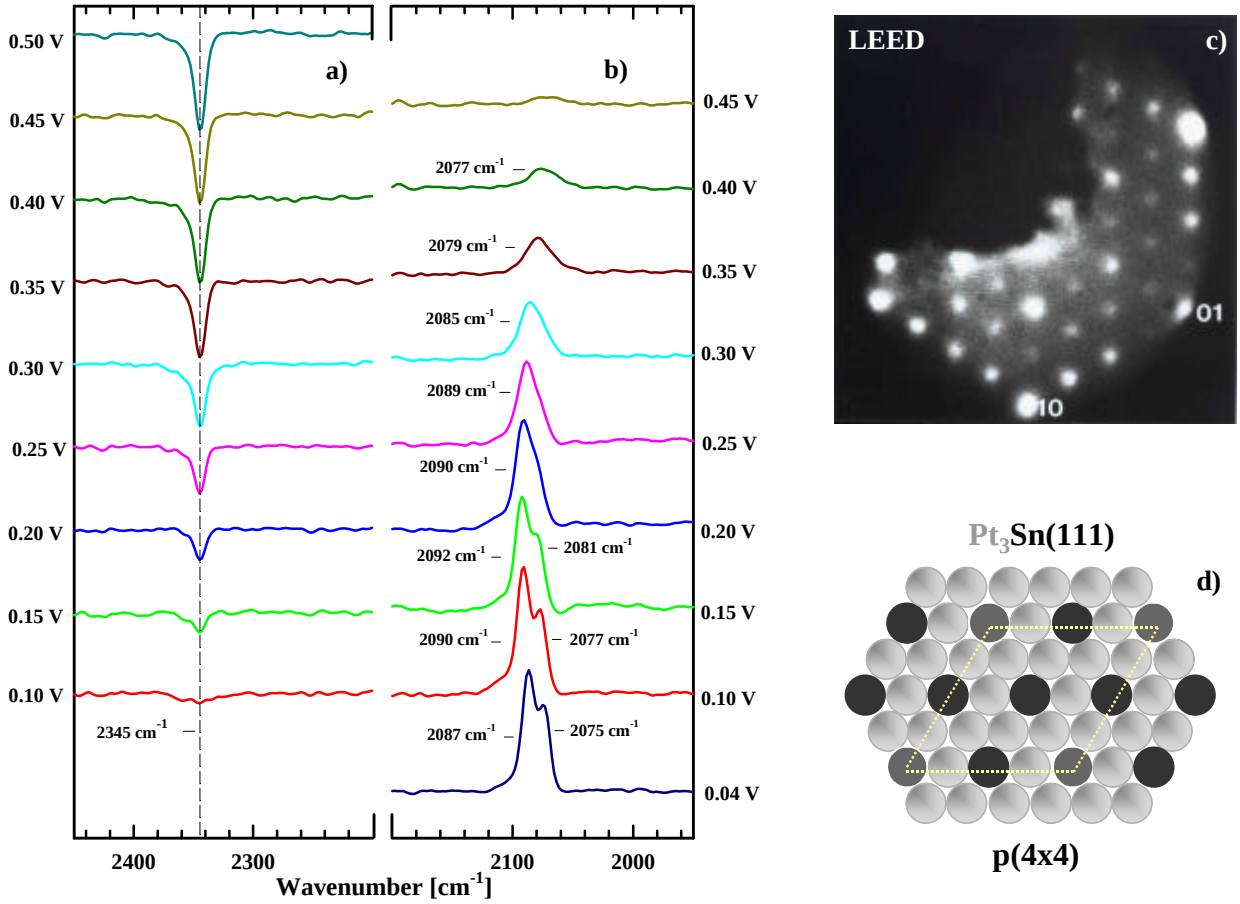

Figure 4. Series of infrared spectra during **(a)** CO_2 production and **(b)** progressive oxidation of CO on $Pt_3Sn(111)$ in 0.5 M H_2SO_4 saturated with CO; each spectrum is accumulated from 50 interferometer scans at the potential indicated. **(c)** LEED pattern and **(d)** schematic representation of the p(4x4) structure observed on $Pt_3Sn(111)$ after expensing surface to O_2. The gray circles are Pt surface atoms, the black circles are Sn atoms covered with OH and dashed circles are Sn atoms which are chemically different from Sn atoms modified with OH.

An illustrative example of the observed differences between CO_{ad} adlayers on Pt(111) and $Pt_3Sn(111)$ is shown in Figure 5, which is a plot of the a-top stretching frequency versus the electrode potential. As shown previously [55], on Pt(111) the linear ν-E plot, with a slope of ca.

30 $cm^{-1}V^{-1}$, is seen prior to occurrence of significant CO oxidation (E > 0.6 V). On $Pt_3Sn(111)$, however, the ν-E slopes for both the high frequency and low frequency CO increase substantially, being ca. 45 $cm^{-1}V^{-1}$ in the potential region just before CO oxidation starts (E > 0.2 V) Observations of the potential effect on the band center in electrochemical experiments are described with equal validity as a change in the extent of $d\pi^*$ metal-CO backbonding [56;57] with applied potential or from a shift of the vibrational frequency from the static electric field of the double layer, the so-called electrochemical Stark effect [58].

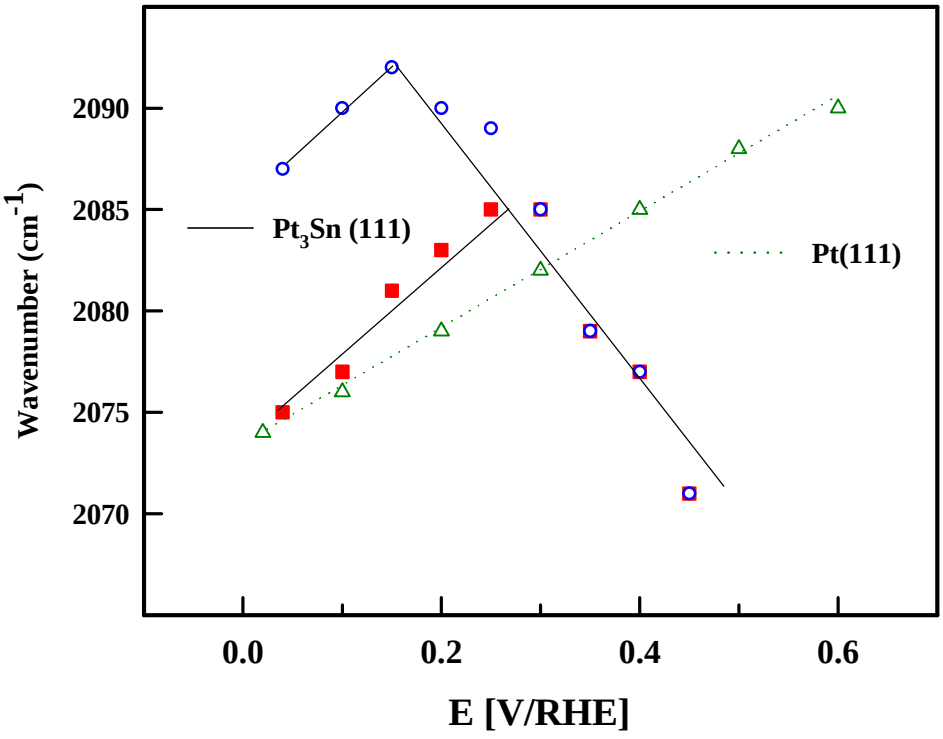

Figure 5. Plots of the peak frequency for the linear CO band vs. the electrode potential on (triangles) Pt(111) and (open circles and squares) $Pt_3Sn(111)$ in 0.5 M H_2SO_4. Data obtained from Figure 4.

Nevertheless, regardless of the exact explanation for how ν depends on E, it is reasonable to assume that the ν-E slopes in an electrochemical environment are dependent on the electrostatic parameters controlled by the applied potential as well as on the substrate-CO energetics. Although there is no straightforward correlation between the C-O stretching

frequency and binding energy [59], the appearance of the higher frequency mode of CO on $Pt_3Sn(111)$ may indicate the formation of a compressed CO adlayer. This layer due to chemical interaction between Pt and Sn atoms (e.g, alloying effects attributed to backdonation of metal electrons into antibonding CO orbitals, which stabilizes the metal-molecule bond and weaker the C-O bond) may lead to the formation of the weakly adsorbed state of CO on Pt sites. Recall that this is in accord with the DFT calculations [48]. In contrast to DFT calculations, however, the most stable adsorption site for CO on the $Pt_3Sn(111)$ surface are the a-top sites. The DFT calculations indicate a preference for the hollow hcp three-fold sites with the Sn atom in the second layer, these sites are preferred over a top site by ca. 0.41 eV. Clearly, the alloying effect alone, which was taken into account in the DFT calculations, cannot accurately predict the potential-induced bandshape/frequency behaviour observed for the CO adlayer on the $Pt_3Sn(111)$ surface. Other factors, such as CO compression into smaller islands, which is governed by intermolecular repulsion, should be taken into account to explain the results in Figure 4b. The phenomenon of island compression is observed in segregated systems where the presence of one species causes the other species to segregate into patches in which the local density is higher than that observed when an equivalent amount of particular species is adsorbed alone [60]. Extending this phenomenon to Figure 4, the presence of oxygenated species on Sn may lead to compression of CO_{ad} molecules resulting in higher local CO coverage that would yield blushifted CO frequencies from the enhanced dipole-dipole coupling. Model calculations indicate than only very small clusters (ca 10 molecules) would be required in order to account for the observed high frequencies on the basis of dipole-dipole coupling [61]. For the $Pt_3Sn(111)$-CO system, the compressive forces can be attributed to the repulsive CO_{ad}-OH_{ad} interaction. The existence of a repulsive CO-O interaction and compression of co-adsorbed CO and O into islands on Pt single crystal surfaces are well

established in UHV experiments and have been discussed independently by Engel and Ertl [62] and White [60].

Although the proposition that the high frequency band is a consequence of mutual interactions between CO_{ad} and OH_{ad} sounds reasonable, it is still puzzling as to why on a monoenergetic surface two-kinds of CO islands can be formed. In general, at the metal-liquid interface the splitting of CO vibrational bands is a fairly universal phenomenon: adsorption of CO on Pt stepped single crystal surfaces covered by submonolayer of CO [63-65], some bimetallic surfaces at which CO is adsorbed on *both* components [66;67] and on more oxophylic metals than Pt, e.g. on a Rh electrode [68] and the Pd(111) surface [69]. Given that SXS results have unambiguously showed that the $Pt_3Sn(111)$ surface is well-ordered and based on the fact that CO is not adsorbed on Sn, one can exclude the first two explanations. Another possible explanation is that Sn exists in two different oxidation states on the $Pt_3Sn(111)$ surface. The hypothesis would be that Co_{ad} adsorbed next to each Sn site would have a unique frequency and potential dependence.

3.5 Oxidation states of Sn: ex-situ LEED/AES

Neither the nature of oxygenated species nor its coverage on Sn atoms is known and none of the *in-situ* spectroscopic techniques we employed were able to resolve this issue. We decided therefore to return to the ex-situ approach, hopping to get in UHV information about the "oxide" formation of Sn atoms. In the UHV experiments, the $Pt_3Sn(111)$ surface was exposed to oxygen and the corresponding structure/chemical changes were monitored by LEED/AES. Dosing the clean annealed surface with oxygen at 4×10^{-8} torr at 300°C produced a sharp p(4 x 4) pattern (Figure 4c) with a Sn/Pt AES ratio of 4.8 (slightly higher than the AES ratio of 4.5 for the p(2 x 2) pattern). These results indicate that chemisorption of oxygen occurs without changing the underlying structure or composition in the $Pt_3Sn(111)$ alloy

surface, consistent with in-situ SXS measurements. The fact that the adsorbed oxygen could only be desorbed by flashing the crystal to 700°C (ca. 100°C higher than for pure Pt)suggests that for the dosing conditions employed in our experiments the oxygen was adsorbed selectively onto Sn sites on the surface. Therefore, the p(4x4) LEED pattern could be interpreted as the adsorption on an oxygen adatom on every other Sn surface atom, as illustrated schematically in Figure 4d.

In what follows, we apply the oxidation results in UHV to an electrochemical environment, assuming that even in electrolyte not every Sn atom is covered with oxygenated species (or at least not with the same-kind of oxygenated species). For simplicity, however, we consider that OH is selectively adsorbed on every second atom and OH-free atoms will be assigned as "non-oxidized" Sn atoms. Under these circumstances, while the high frequency CO_{ad} may occupy Pt atoms which are adjacent to "OH_{ad}"-covered Sn atoms (black circles in the model of Figure 4d), the low frequency CO may occupy Pt sites in the vicinity of "non-oxidized" Sn atoms (shade circles in the model of Figure 4d). Recall that in the former case the repulsive CO_{ad}-OH_{ad} interaction leads to formation of cluster domains where the local CO coverage within such patches remain higher than in the latter case.

3.6 Time resolved FTIR spectroscopy of CO oxidation

Figures 6a and 6b show that the oxidative removal of CO_{ad} from the $Pt_3Sn(111)$ surface, established by monitoring the concomitant development of the asymmetric O-C-O stretch of dissolved CO_2 at 2343 cm^{-1}, starts as low as at 0.1 V. Plots of the integrated intensities of the adsorbed CO stretching band (I_{CO}) and the integrated intensities for CO_2 production (I_{CO2}) as a function of electrode potential in CO saturated 0.5 M H_2SO_4 solution are summarized in Figure 6c. Clearly, I_{CO2}-E and I_{CO}-E plots show that the decrease in the CO intensity is mirrored by an increase in CO_2 production, consistent with the L-H mechanism

(Eq.1) proposed above. Notice that although the oxidative removal of CO starts at very low potentials (ca 0.1 V in Figure 4), the slope of the I_{CO2}-E and I_{CO}-E plots are rather small, at least compared to the corresponding plots for CO oxidation on Pt(111) in acid solutions [50]. This suggests that the turn over frequency, defined as the number of complete reaction events per active sites per second, for CO oxidation on $Pt_3Sn(111)$ is low relative to Pt(111) at potentials where there is nucleation of the OH_{ad} on both surfaces.

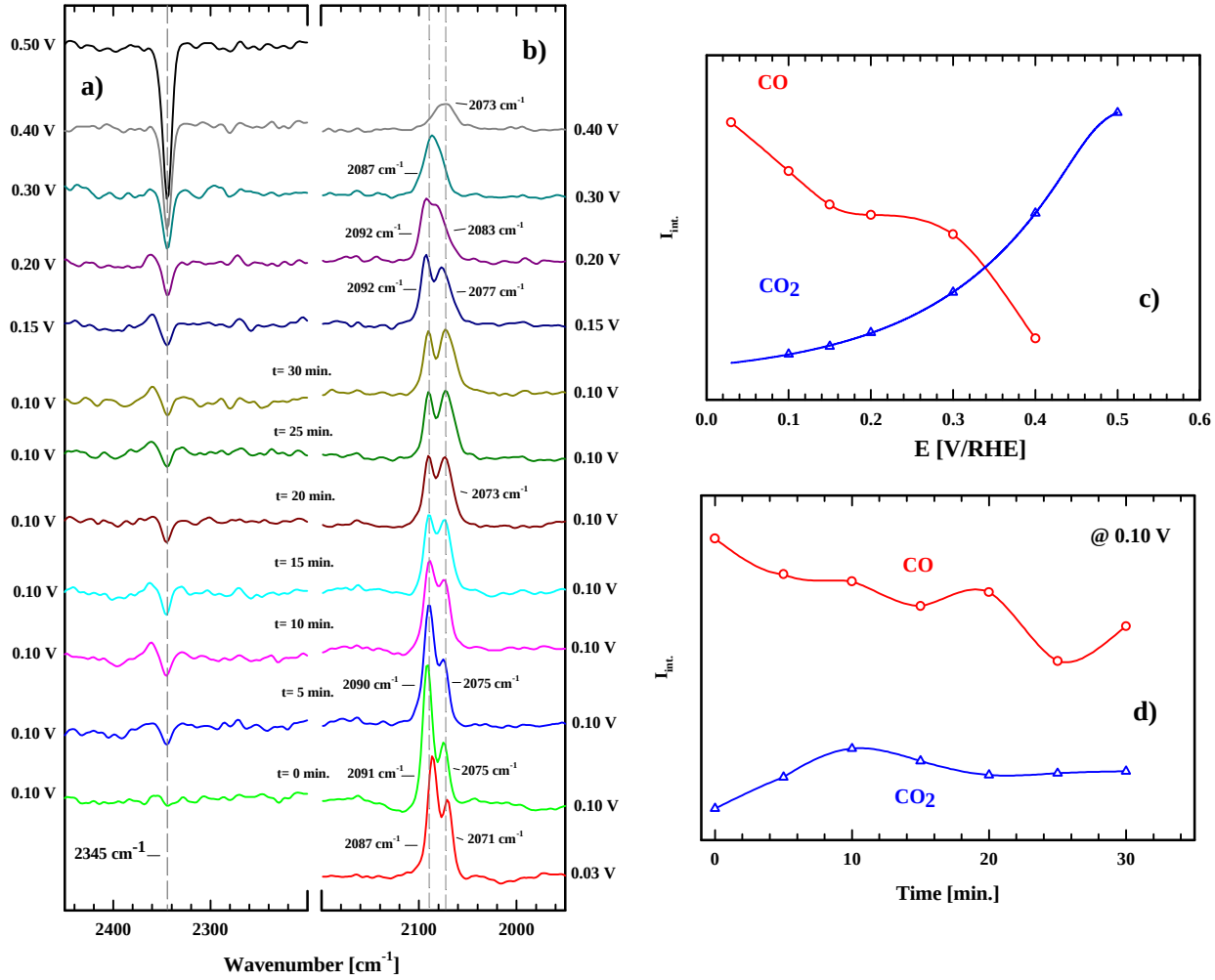

Figure 6. Time resolved FTIR spectra for **(a)** CO_2 production and **(b)** CO band morphology at different potentials. **(c)** Integrated intensities for CO_2 production and CO_{ad} as a function of electrode potential in CO-saturated 0.5 M H_2SO_4 solution. **(d)** Integrated intensities for CO_2 production and CO_{ad} as a function of time in CO-saturated 0.5 M H_2SO_4 solution.

The lower turnover rate on the former surface is possibly due to stronger adsorption and lower reactivity of the OH_{ad} on the Sn site versus Pt. Nevertheless, in general, the rate of CO oxidation on $Pt_3Sn(111)$ depends on the delicate balance between the rate of re-adsorption (k_{ad}) of CO_b on Pt sites created each time that CO_{ad} is oxidized (k_{ox}) in the L-H type reaction (Eq.1),

$$CO_b \xrightarrow{k_{ad}} CO_{ad} \xrightarrow{k_{ox}} CO_2 \xrightarrow{k_d} CO_{2,b} \qquad (2)$$

In FTIR experiments, if one takes into account that CO_2 may slowly diffuse out of the thin-layer cell (CO_{2b}), then k_d in reaction scheme (2) represents the rate of this diffusion. In order to see this balance in action, time-dependent changes in integrated intensities of CO_{ad} and CO_2 are monitored at constant potentials. Figure 6 shows a clear trend that while I_{CO} decreases with time (τ) I_{CO2} has a tendency to increase with time, consistent with the L-H mechanism and continuous oxidation of CO even at this low potential. As discussed in our recent papers [15], it turns out that this small activity is an important property for CO-tolerant catalysts. Closer examination of Figure 6d, however, reveals some time-dependent deviations, e.g. I_{CO2} first increases with time, reaching the maximum after ca. 10 min., and then, after a small decrease in I_{CO2}, the production of CO_2 reaches the steady state value for $\tau > 20$ min. To explain this we return to reaction scheme (2), which describes the possible reaction steps in the thin layer cell. Considering that I_{CO2} is controlled by the delicate balance between the time-dependent diffusion of CO_2 out of the thin layer cell (k_d) and the production of CO_2, the latter being controlled simultaneously by the relation between k_{ad} and k_{ox}, we suggest that after the first 10 min $k_{ad} + k_{ox} < k_d$, for $10 < \tau < 20$ min. $k_d < k_{ad} + k_{ox}$ and, finally, after ca 20 min CO_2, production probed by IR beam remains constant ($k_{ad} + k_{ox} = k_d$).

Another result from the time-resolved FTIR spectroscopy is the change in the morphology of CO stretching bands with time. Figure 6 shows that initially (E=0.1 V and τ=0)

the high frequency band of atop CO has much higher intensity than the low frequency band of atop CO. As time increases, the former band become less intense and after ca. 30 min. the band intensity for high frequency CO and low frequency CO become the same. This behavior indicates that the oxidative removal of CO at low potentials proceeds first on the surface sites where local (microscopic) CO coverage remains high and thus CO is weakly adsorbed on Pt. Linking the microscopic and macroscopic levels of characterization, the weakly adsorbed (CO_{ad}^{w}) state may correspond microscopically to the formation of disordered but compressed CO patches with characteristic high frequency a-top CO IR bands. Furthermore, Figures 4 and 6 reveal that pair of bands (centered at ca. 2090 and 2077 cm^{1-}) at 0.1 V are transformed into a single relatively broad peak centered at ca. 2077 cm^{-1} at higher potentials. It is this relaxed CO adlayer with a low vibrational frequency which was previously characterized as the strongly adsorbed state of CO_{ad} [20].

4. Conclusions:

In situ studies by surface X-ray scattering (SXS) and Fourier transform infrared (FTIR) spectroscopy are used to create a link between the detailed structure/composition of a $Pt_3Sn(111)$ surface in an electrochemical environment and the macroscopic kinetic rates of the reacting system. The $Pt_3Sn(111)$ single crystal electrode was prepared and characterized in UHV prior to transfer into electrochemical cells. In agreement with previous work, the clean-annealed surface produced half-order spots in the LEED pattern, forming the p(2 x 2) structure which is consistent with the surface composition, determined by LEIS, of 25 at% Sn.

SXS results showed that the p(2 x 2) structure can be transferred from UHV into 0.5 M H_2SO_4 using the procedures developed in this laboratory. This structure remains stable, with the surface composition expected for the bulk termination, upon repeated potential cycling from 0.05 to 0.8 V. Adsorption of sulfuric acid anions on the p(2 x 2) phase, which was

studied by FTIR, produced a characteristic 'butterfly-like feature in the CV of $Pt_3Sn(111)$. Detailed analysis of the SXS results revealed that expansion of surface atoms at 0.05 V, induced by adsorption of hydrogen, is ca. +2% from the bulk lattice spacing. At 0.5 V, where there is no hydrogen adsorption, the Pt atoms occupy bulk lattice positions but Sn atoms expand significantly, ca 8.5%, i.e. there is significant buckeling of the topmost atomic layer. SXS results also showed that the p(2 x 2) structure is stable in a solution containing CO. In contrast to the Pt(111)-CO system, however, no ordered structures of CO were observed on the $Pt_3Sn(111)$ surface and Pt in the topmost layer expands relatively little (ca. 1.5%) from the bulk lattice spacing upon the adsorption of CO, i.e. significantly smaller than the 4% expansion observed upon the adsorption of CO on Pt(111). The difference in relaxation of these two surfaces covered by CO probably arises from the difference in the metal-adsorbate bonding, the Pt(111)-CO interaction being stronger than the $Pt_3Sn(111)$-CO interaction. The binding site geometry of CO on $Pt_3Sn(111)$ was determined by FTIR. In contrast to the near invariant band of a-top CO on Pt(111), changes in bandshape (splitting of the band) and frequency (increase in the frequency mode) are clearly visible on the $Pt_3Sn(111)$ surface. In order to explain the lineshape of CO bands we suggest that, in addition to alloying effecting other factors, such as intermolecular repulsion between coadsorbed spaces, Sn atoms exists in two different chemical forms in the $Pt_3Sn(111)$ surface and the high frequency CO_{ad} occupies Pt atoms which are adjacent to "OH_{ad}"-covered Sn atoms, the low frequency CO may occupy Pt sites in the vicinity of "non-oxidized" Sn atoms. The weakly adsorbed and more reactive form of CO_{ad} is that adsorbed next to the "OH_{ad}"-covered Sn atoms. Because of the weak adsorption, these sites are occupied only at high surface coverage of CO_{ad}, giving rise to a positive reaction order in p_{CO} for continuous oxidation of CO_b in solution.

Acknowledgement.

This work was supported by the Director, Office of Science, Office of Basic Energy Sciences, Division of Materials Sciences, U.S. Department of Energy under Contract No. DE-AC03-76SF00098.

References

(1) Samant, M. G.; Toney, M. F.; Borges, G. L.; Blurton, K. F.; Melroy, O. R. *J.Phys.Chem.* **1988**, *92*, 220.

(2) Ocko, B. M.; Wang, J.; Davenport, A.; Isaacs, H. *Phys.Rev.Lett.* **1990**, *65*, 1466-1469.

(3) Toney, M. F.; Ocko, B. M. *Synchrotron Radiation News* **1993**, *6*, 28-33.

(4) Tidswell, I. M.; Markovic, N. M.; Ross, P. N. *Phys.Rev.Lett.* **1993**, *71*, 1601-1604.

(5) Lucas, C.; Markovic, N. M.; Ross, P. N. *Surf.Sci.* **1996**, *340*, L949-L954.

(6) Lucas, C.; Markovic, N. M.; Ross, P. N. *Phys.Rev.Lett.* **1996**, *77*, 4922-4925.

(7) Itaya, K. *Progress in Surface Science* **1998**, *58*, 121-247.

(8) Kolb, D. M. *Progress in Surface Science* **1996**, *51*, 109-173.

(9) Faguy, P. W.; Markovic, N.; Adzic, R. R.; Fierro, C. A.; Yeager, E. B. *J.Electroanal.Chem.* **1990**, *289*, 245-262.

(10) Nichols, R. J. Imaging Metal Electroctrocrystallization at High Resolution; In *Frontiers of Electrochemistry;* Lipkowski, J., Ross, P. N., eds. Wiley-VCH,Inc: New York, 1999; pp 99-137.

(11) Sawatari, Y.; Inukai, J.; Ito, M. *J.Electron Spec.* **1993**, *64/65*, 515-522.

(12) Nart, F. C.; Iwasita, T.; Weber, M. *Electrochim.Acta* **1994**, *39*, 961.

(13) Pleskov, Y. V.; Filinovskij, V. Y. *The Rotating Disc Electrode*; Consultant Bureau: New York, 1976.

(14) Bard, A. J.; Faulkner, L. R. *Electrochemical Methods*; Wiley & Sons: New York, 1980; p 283.

(15) Markovic, N. M.; Ross, P. N. *Surf.Sci.Reports* **2002**, *45*, 121-254.

(16) Watanabe, M.; Motoo, S. *J.Electroanal.Chem.* **1975**, *60*, 259-266.

(17) Watanabe, M.; Motoo, S. *J.Electroanal.Chem.* **1975**, *60*, 275-283.

(18) Gasteiger, H. A.; Markovic, N.; Ross, P. N.; Cairns, E. J. *J.Phys.Chem.* **1994**, *98*, 617-625.

(19) Gasteiger, H. A.; Markovic, N. M.; Ross, P. N. *J.Phys.Chem.* **1995**, *99*, 8945-8949.

(20) Gasteiger, H. A.; Markovic, N. M.; Ross Jr., P. N. *Catal.Let.* **1996**, *36*, 1-8.

(21) Haner, A. N.; Ross, P. N.; Bardi, U. *Surf.Sci.* **1991**, *249*, 15-20.

(22) Ferrero, R.; Capelli, R.; Borsese, A.; Delfino, S. *Atti.Accad.Naz.Lincei Red.Cl.Sci.Fis.Mat.Nat.* **1973**, *54*, 634.

(23) Taglauer, E.; Heiland, W. *Applied Surface Analysis* **1980**, *669*, 111-124.

(24) Gasteiger, H. A.; Markovic, N.; Ross, P. N.; Cairns, E. J. *J.Phys.Chem.* **1993**, *97*, 12020-12029.

(25) Markovic, N. M.; Grgur, B. N.; Ross Jr., P. N. *J.Phys.Chem.B* **1997**, *101*, 5405-5413.

(26) Lucas, C. A.; Markovic, N. M.; Grgur, B. N.; Ross Jr., P. N. *Surf.Sci.* **2000**, *448*, 65-76.

(27) Clavilier, J. *J.Electroanal.Chem.* **1980**, *107*, 211-216.

(28) Markovic, N. M.; Hanson, M.; McDougal, G.; Yeager, E. *J.Electroanal.Chem.* **1986**, *241*, 309.

(29) Zelenay, P.; Wieckowski, A. *J.Electrochem.Soc.* **1992**, *139*, 2552-2558.

(30) Kolics, A.; Wieckowski, A. *J.Phys.Chem.B* **2001**, *105*, 2588-2595.

(31) Savich, W.; Sun, S. G.; Lipkowski, J.; Wieckowski, A. *J.Electroanal.Chem.* **1995**, *388*, 233-237.

(32) Funtikov, A. M.; Stimming, U.; Vogel, R. *J.Electroanal.Chem.* **1997**, *482*, 147-153.

(33) Markovic, N. M.; Marinkovic, N. S.; Adzic, R. R. *J.Electroanal.Chem.* **1988**, *241*, 309.

(34) Varga, P.; Zelenay, P.; Wieckowski, A. *J.Electroanal.Chem.* **1992**, *330*, 453-467.

(35) Shi, Z.; Lipkowski, J. *J.Electroanal.Chem.* **1994**, *364*, 289-294.

(36) Wu, S.; Shi, Z.; Lipkowski, J.; Hitchcock, A. P.; Tyliszczak, T. *J.Phys.Chem.* **1997**, 10310-10322.

(37) Markovic, N.; Ross, P. N. *Langmuir* **1993**, *9*, 580-590.

(38) Markovic, N.; Gasteiger, H. A.; Ross, P. N. *Langmuir* **1995**, *11*, 4098-4108.

(39) Markovic, N. M.; Grgur, B. N.; Lucas, C.; Ross, P. N. *J.Chem.Soc.Faraday Trans.* **1998**, *94*, 3373-3379.

(40) Schmidt, T. J.; Markovic, N. M.; Ross, P. N. *J.Phys.Chem.B* **2001**, *67*, 1.

(41) Markovic, N. M.; Ross, P. N. *J.Electroanal.Chem.* **1992**, *330*, 499-520.

(42) Schmidt, T. J., Stamenkovic, V. R., Lucas, C. A., Markovic, N. M. and Ross Jr., *Phys.Chem.Chem.Phys.*, **2001**, 3, 3879-3890.

(43) Schmidt, T. J.; Grgur, B. N.; Markovic, N. M.; Ross Jr., P. N. *J.Electroanal.Chem.* **2001**, *500*, 36-43.

(44) Stamenkovic, V.; Markovic, N. M. *Langmuir* **2000**, *17*, 2388-2394.

(45) Feidenhans'l *Surf.Sci.Reports* **1989**, *10*, 105-188.

(46) Lucas, C. A.; Markovic, N. M.; Ross, P. N. *Surf.Sci.* **1999**, *425*, L381-L386.

(47) Tidswell, I. M.; Markovic, N. M.; Ross, P. N. *J.Electroanal.Chem.* **1994**, *376*, 119-126.

(48) Shubina, T. E.; Koper, M. T. M. *Electrochima Acta* **2002**, *47*, 3621-3628.

(49) Markovic, N. M.; Grgur, B. N.; Lucas, C. A.; Ross, P. N. *J.Phys.Chem.B* **1999**, *103*, 487-495.

(50) Markovic, N. M.; Lucas, C. A.; Rodes, A.; Stamenkovic, V.; Ross, P. N. *Surf.Sci.Lett.* **2002**, *499*, L149-L158.

(51) Kitamura, T.; Takahashi, M.; Ito, M. *Surf.Sci.* **1989**, *358*, 337.

(52) Villegas, I.; Weaver, M. J. *J.Chem.Phys.* **1994**, *101*, 1648.

(53) Iwasita, T.; Nart, F. C. *Progress in Surface Science* **1997**, *55*, 271-340.

(54) Rodes, A.; Gomez, R.; Feliu, J. M.; Weaver, M. J. *Langmuir* **2001**, *16*, 811-816.

(55) Chang, S. C.; Weaver, M. J. *J.Phys.Chem.* **1990**, 4582.

(56) Holloway, S.; Norskov, J. K. *J.Electroanal.Chem.* **1984**, *101*, 193.

(57) Anderson, A. B. *J.Electroanal.Chem.* **1990**, *280*, 37.

(58) Lambert, D. K. *Electrochim.Acta* **1995**, *41*, 623-630.

(59) Koper, M.; van Santen, R. A.; Wasileski , S. A.; Weaver, M. J. *J.Chem.Phys.* **2000**, *113*, 4392-4407.

(60) White, J. M.; Akhter, S. Adsorbate-Adsorbate Interactions During Coadsorption on Metals; In *Crit.Rev.Solid State Mater.Sci*; CRC: 1988; pp 131-173.

(61) Severson, M. W.; Stuhlmann, C.; Villegas, I.; Weaver, M. J. *J.Chem.Phys.* **1995**, *103*, 9832-9843.

(62) Engel, T.; Ertl, G. *Adv.Catal.* **1979**, *28*, 1.

(63) Kim, C. S.; Korzeniewski, C.; Tornquist, W. J. *J.Chem.Phys.* **1993**, *100*, 628-630.

(64) Kim, C. S.; Tornquist, W. J.; Korzeniewski, C. *J.Chem.Phys.* **1994**, *101*, 9113-9121.

(65) Kim, C. S.; Korzeniewski, C. *Anal.Chem.* **1997**, *69*, 2349-2353.

(66) Friedrich, K. A.; Geyzers, K.-P.; Linke, U.; Stimming, U.; Stumper, J. *J.Electroanal.Chem.* **1996**, *402*, 123-128.

(67) Arenz, M.; Stamenkovic, V.; Wandelt, K.; Ross, P. N.; Markovic, N. M. *Surf.Sci.* **2002**, *506*, 287-296.

(68) Lin, W.-F.; Sun, S. G. *Electrochim.Acta* **1996**, *41*, 803-809.

(69) Zou, S.; Gomer, R.; Weaver, M. J. *J.Electroanal.Chem.* **2002**, *474*, 155-166.

(70) Faguy, P. W.; Marinkovic, N. S.; Adzic, R. R. *J.Electroanal.Chem.* **1996**, *407*, 209-218.

Table of Contents Graphic